Ray-optical simulation of the static and dynamic transfer behavior of PCB-integrated optical interconnects

December 19, 2005

Abstract

Printed-Circuit-Board (PCB) integrated optical waveguides possess the capability to overcome the arising bandwidth bottleneck of on-board, inter-chip interconnects. In order to meet the requirements of the PCB technology, highly multimode optical waveguides integrated within the PCB are currently object of international research activities. Beyond adequate manufacturing processes, the industrial scale application of this innovative technology requires efficient design and simulation tool, which his paper is dealing with.

1 Introduction

According to Moores's law the clock speed within and between high performance electronic systems will increase up to 10 Gbps in the year 2010 [1]. This requires new concepts for on-board, interchip interconnects as the conventional electrical interconnects are increasingly facing EMC problems at this high clock speeds.
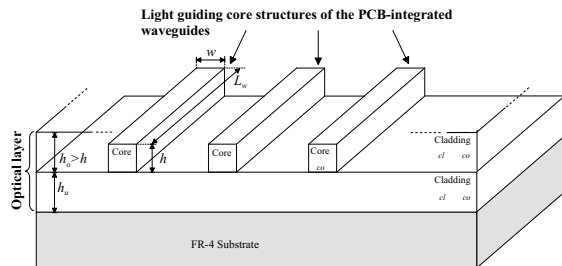

Figure 1: Optical layer with buried light guiding core structures of PCB-integrated waveguides

A promising approach to overcome the interconnect bottleneck problem is to replace conventional copper interconnects with optical interconnects [3], [7]. Their high bandwidth capability is well adapted to the needs of future high speed inter-chip interconnects [2]. As the integration of optical interconnects into conventional PCBs requires compatibility with existing PCB manufacturing processes, a new technology for PCB-based optical interconnects is currently under development (e. g. [10], [5]). A typical implementation of this technology can be described as follows: By applying hot embossing, photo-lithographic methods or laser direct writing, light guiding, polymer core structures are integrated into a polymer optical layer. The polymer layer with lower material permittivity $\epsilon_{cl} < \epsilon_{co}$ compared to the core structure represents the cladding of the optical waveguide, required for light guidance. Based on the manufacturing methods, the light guiding core structures are optically homogeneous and show a constant rectangular cross section (see Fig. 1) along their axis. With this integrated optical waveguides, the same degree of freedom in routing optical interconnects as conventional electrical ones is achieved. By laminating the optical layer into a multi-layer board, a conventional PCB-system is supplemented with high speed optical interconnects. Furthermore chip packaging and assembly techniques are currently under development, providing the PCB system with VCSELs used as transmitting and photodiodes as receiving components. The optical coupling between the transmitting and receiving components and the optical waveguides is realized by free-space optics and 45-deflection mirrors or butt-coupling arrangement. In order to avoid active alignment for the optical transceiver and receiver modules, the core cross sectional dimensions of the integrated optical waveguides are in the range of conventional micro strip lines ($100 \times 100 \mu m^2$). Thus their dimensions meet the accuracy requirements ± 25 to $\pm 50 \mu m$ [9], [6] of automatic pick and place equipment.

Apart from technological aspects there is also a need for optical design and simulation tools [10]. At present the design of electronic components and systems is entirely based on software tools. Especially for the design of electrical interconnects for PCBs there exist a lot of EDA tools. Consequently the industrial scale application of PCB-integrated optical waveguides will require efficient optical design and simulation tools as well. As comparable tools for the new optical interconnect technology do not exist, an adapted computer-aided design and ray-optical simulation tool for PCB-integrated optical waveguides was developed and implemented. The novel optical design technique enables a user-friendly design and analytical description of almost arbitrarily shaped 3-D boundary geometries of light guiding core structures of integrated optical waveguides. Furthermore the analytical description of the core geometry comes along with efficient, analytical algorithms for fast ray intersection point computations with plane and curved core boundaries. Both the analytical description of the 3-D geometry of the core boundary as well as the ray intersection algorithms provides the basis for ray-optical analysis. The introduced ray-optical simulation tool computes the optical wave propagation along afore designed core boundaries under consideration of various launch conditions and specific waveguide properties. It combines ray-tracing techniques based on the laws of geometrical optics with wave optical models to describe the interaction of rays at core boundaries. In combination both tools enable the user to compute and ana-

lyze the static and dynamic optical transfer behavior of PCB-integrated waveguides. In this context the static transfer behavior describes basically the loss behavior of the waveguide caused by intrinsic material losses, radiation losses due to nano-rough core boundaries or poorly designed core structures. Complementing the static transfer behavior, the dynamic one specifies the time response of optical waveguides, which is derived by computing their characteristic step responses. Based on the step response, characteristic time domain properties like signal delay, dispersion, skew and rise/fall time are derived.

2 Design of optical interconnects

The application of the ray-optical simulation method for PCB-integrated optical waveguides requires the geometrical description of the core boundary, which is obtained by the subsequently introduced design technique. This novel technique must provide an analytical description of the 3-D core boundary geometry under consideration of a user-friendly design process. The design process is subdivided into two manual 2-D design steps for the core's cross sectional contour and the core's routing within the optical plane. Based on the two manual designs, the design technique provides an algebraic description of the core's boundary geometry. The algebraic nature of the description is a precondition for an efficient ray-optical simulation, as it enables an analytical and thus fast determination of ray intersection points with the core boundary. In regard to the high amount of ray intersection calculations, which have to be carried out during the simulation process, this design constraint is essential. In order to obtain analytical ray intersection calculation algorithms, another constraint has to be met: The surface elements of the core boundary must be of the first or second geometrical order. This requirement restricts the core's routing to rectilinear or circular bended routing sections.

The 2-D design of the cross sectional contour of the core structure is done by specifying a finite set of in-plane vectors $\boldsymbol{Q}_i$, spanning up the contour. By applying parameterized vector functions $\boldsymbol{Q}_i(t)$, which define the rectilinear contour curve between two adjacent vectors, a closed parameterized vector curve can be derived to describe the contour analytically.

$$\boldsymbol{Q}(t) = \sum_{i=0}^{N_Q-1} \boldsymbol{Q}_i(t) \quad \text{with } \boldsymbol{Q}_i(t) \cdot \boldsymbol{e}_y = 0 \qquad (1)$$

The 2-D design of the routing trajectory of the core structure starts with the definition of a placement vector $\boldsymbol{A}_0$ and a tangent vector $\boldsymbol{T}_0$ within the xy-plane. Based on these two vectors and sequentially selected design parameters radius and arc length for bended routing sections or length for rectilinear routing sections, a continuously differentiable routing trajectory is computed by the design technique. The derived routing trajectory $\boldsymbol{A}(s)$ is algebraically described in sections by a set of parameterized vector functions $\boldsymbol{A}_j(s)$:

$$\boldsymbol{A}(s) = \sum_{j=0}^{N_A-1} \boldsymbol{A}_j(s) \quad \text{with } \boldsymbol{A}_j(s) \cdot \boldsymbol{e}_z = 0 \qquad (2)$$

The computed routing trajectory for a design example with $N_A = 10$ is given in Fig. 2. In order to obtain the
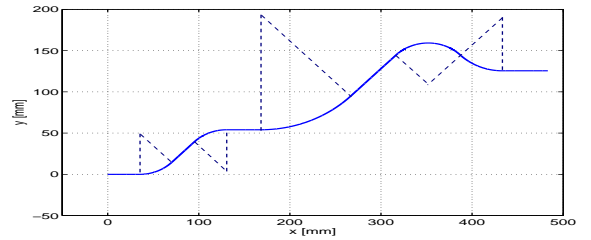

Figure 2: Designed routing trajectory $\boldsymbol{A}(s)$

algebraic description of the 3-D core boundary geometry another set of parameterized vector functions is required, which describe the tangent vector along the routing trajectory.

$$\boldsymbol{T}_j(s) = \frac{\partial \boldsymbol{A}_j(s)}{\partial s} \quad \text{with} |\boldsymbol{T}_j(s)| = 1 \qquad (3)$$

By applying the parameterized vector functions (1), (2) and (3), the 3-D geometry of the core boundary is algebraically described in sections by another set of parameterized vector functions:

$$\boldsymbol{H}_{ij}(s,t) = [T_{jy}(s)Q_{ix}(t), -T_{jx}(s)Q_{ix}(t), Q_{iz}(t)]^T \quad (4)$$
$$+ \boldsymbol{A}_j(s)$$

With this set of parameterized vector functions each position on the core boundary is described analytically. Applying this technique the 3-D geometry for slight
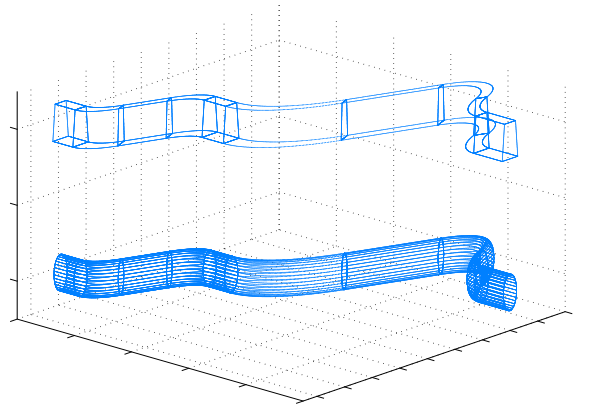

Figure 3: 3-D geometry of the core boundary

trapezoidal and circular cross sections is computed on the basis of the routing trajectory depicted in Fig. 2 and visualized in Fig. 3. For evaluating the Fresnel equations and wave optical scattering model, the angle of incidence must be known, which is spanned by the ray propagation direction and the surface normal of the boundary at the intersection point. Therefore a further set of parametric vector functions is introduced that

$$\boldsymbol{N}_{ij}(s,t) = \boldsymbol{T}_j(s) \times \frac{\partial \boldsymbol{H}_{ij}(s,t)}{\partial t} \qquad (5)$$

describe the surface normal at any point of the core boundary. Due to the algebraic description of the boundary and the restriction to rectilinear or circular

bended routing sections, the ray intersection calculation for rectilinear ray paths with the core boundary is achieved by solving the linear or quadratic equation system analytically:

$$\boldsymbol{H}_{ij}(s,t) - (\boldsymbol{S}_0 + u\,\boldsymbol{S}) = \boldsymbol{0} \;\Rightarrow\; (s_0, t_0, u_0). \quad (6)$$

This equation system must be solved for all surface elements $i \in [0, N_Q - 1]$ and $j \in [0, N_A - 1]$. If the derived surface intersection parameters s_0, t_0 are within the definition range $[0, 1]$ and the ray parameter u_0 represents the smallest positive parameter, the intersection point $\tilde{\boldsymbol{S}}_0$ is given by:

$$\tilde{\boldsymbol{S}}_0 = \boldsymbol{S}_0 + u_0\,\boldsymbol{S} \quad \text{with } u_0 > 0. \quad (7)$$

Integrating this intersection algorithm into a ray-tracing technique and considering Snell's law of reflection at each intersection point, the geometrical ray path can be computed along the core structure of a PCB-integrated waveguide. An example of a propagating ray path with 44 reflection points is given in Fig. 4. In order to compute the ray path 704 ray intersection calculations had to be made.
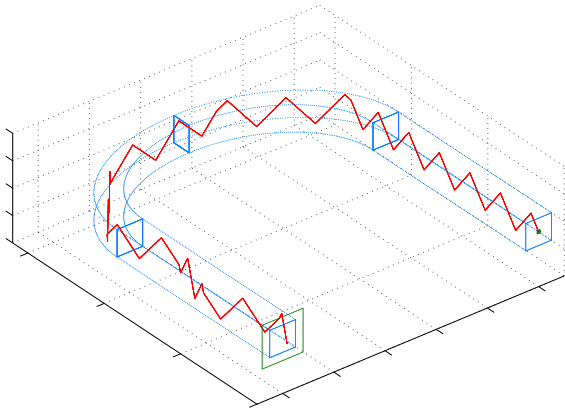

Figure 4: Geometrcial ray path propagating along a designed core structure

For visualization purposes in Fig. 4 the transversal dimensions of the core are chosen to be large compared to its axial length, resulting in a much smaller number of reflection points along a ray path. For real-life PCB-integrated optical waveguides, the transversal core dimension are much smaller (factor $0.01 - 0.0001$) compared to their axial dimensions.

3   Hybrid ray-optical method

In contrast to high frequency electrical interconnects, the electromagnetic field propagating along an optical waveguide is concentrated on its core region. Thus the numerical calculation of optical wave propagation can be limited to the inner core region of the waveguide. As the transversal core dimensions of the PCB-integrated waveguides are large compared to the targeted optical wavelength ($0.65\mu m$ up to $0.95\mu m$), the discrete electro-magnetic guided mode-spectrum is merging into a quasi-continuous mode spectrum. This allows the application of a hybrid ray-tracing method based on the laws of geometrical optics [11], [8]. In order to compute

guided wave propagation by ray-tracing, the behavior of local plane waves

$$\underline{\boldsymbol{E}}(\boldsymbol{r}) = \underline{\boldsymbol{E}}_0\,e^{-j(\underline{\boldsymbol{k}}\cdot\boldsymbol{r} - \omega t)} \quad \text{with } \underline{\boldsymbol{k}} = \omega\sqrt{\underline{\epsilon}_{co}}\,c_0^{-1} \wedge \underline{\boldsymbol{k}} \,\|\, \boldsymbol{S} \quad (8)$$

and their properties (field energy, polarization, optical path length) are assigned to the ray path. As the polymer core structures are homogeneous in terms of their permittivity $\underline{\epsilon}_{co} \neq f(\boldsymbol{r})$, rays are propagating along rectilinear paths throughout the core media satisfying the eikonal equation of geometrical optics [11]. Due to lossy polymer core material, the amount of field energy of the local plane wave traced along the ray path, must be reduced. This energy reduction can be considered within the ray-optical method by introducing a complex core permittivity with a slight electric conductivity κ.

$$\underline{\epsilon}_{co} = \left(\epsilon_{co} - j\frac{\kappa}{\omega\epsilon_0}\right) \quad \text{with } \frac{\kappa}{\omega\epsilon_0} \ll \epsilon_{co} \quad (9)$$

The imaginary part of the core permittivity leads to a field reduction of the local plane wave (8) and consequently causes an energy reduction along the ray path. When striking a core boundary rays are specular reflected by satisfying Snell's law [8]. The amount of power of the specular reflected ray is defined by the Fresnel equations [8]. Depending on these equations that are parameterized by the angle of incidence and the real parts of the permittivity on both sides of the core's boundary, the ray is partially or totally reflected. In order to take intrinsic material losses of the covering cladding material into account, the Fresnel equations can be evaluated using the complex cladding permittivity instead of its real part [8]. This leads to a slight reduction of the reflected power even if the ray is totally reflected. By extending Fresnel reflection by local scattering processes, the influence of manufacturing based nanorough core boundaries can be integrated into ray-optical simulation as well [4]. This leads to a slight decrease of field energy of the specular reflected ray. The lost field energy of the specular reflected ray is transferred into a spectrum of refractive and reflective scattered rays. While the first one causes radiation loss the latter one leads to scattered rays, which have to be traced throughout the waveguide as well. As the axial dimensions of the waveguides are large compared to their transversal dimensions, ray paths undergo a high number (> 100) of local reflection or scattering processes at which they lose a fraction of their incident field energy. Thus only ray paths that undergo total internal reflection at each boundary intersection contribute to wave propagation along the waveguide.

In contrast to high frequency electrical interconnects the static and dynamic transfer behavior of PCB-integrated waveguides strongly depends on the initial launch condition of the optical source. This is explained by the fact that each ray path has its own characteristic propagation time and loss behavior. Thus each optical simulation of the transfer behavior must consider a specific launch condition. This can be achieved by applying ray-optical source models. They convert a scalar signal (e.g. step function) into a spatial light emission spectrum, which can be emulated by a discrete set of local plane waves. These plane waves serve to initialize the ray-tracing algorithm and are traced along the core structure of the designed waveguide. In order to evaluate the static and dynamic transfer behavior of the waveguide, the field energy of the local plane waves

traced along the ray paths has to be converted back into a scalar signal. Therefore so-called virtual detectors are introduced, which are represented each by a spatial limited plane placed at specified positions along the waveguide. They record the optical field energy and delay time of each incident ray and compute a scalar step response by integrating time sorted field energy fractions $P_D(\tau)$ of all detected rays over the time.

$$\sigma(t) = \frac{1}{P_Q} \int_{T_0}^{t} P_D(\tau)\, d\tau \quad \text{and } t \in [T_0, T_0 + T_D] \quad (10)$$

As exemplarily depicted in Fig. 5, derived step responses always show a monotonically increasing curve progression. By normalizing the step response to the optical power P_Q emitted by the applied source, the final value of the step response represents the signal attenuation. For perfect optical transmission without any appearing losses, the final value of the step response always reaches unity. Introducing detector thresholds
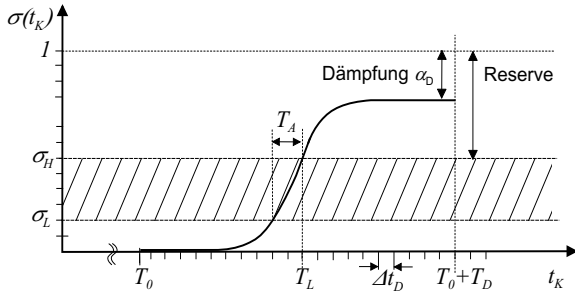

Figure 5: Optical step response and evaluation criteria

P_{DH}, P_{DL} for certain switching operation, the power budget as well as timing criteria can be evaluated. In order to integrate the absolute values of the switching thresholds into the step response representation (10), they have to be normalized to the source power P_Q.

$$\sigma_H = \left.\frac{P_{DH}}{P_Q}\right|_{0\to1} \wedge \sigma_L = \left.\frac{P_{DL}}{P_Q}\right|_{1\to0} \quad (11)$$

For proper operation the optical loss must be smaller than the power budget. The dynamic evaluation of the step response includes the offset delay time T_0, the dispersion time T_D, the signal delay time T_L an the rise time T_A. The offset delay time is defined by the point in time, at which the first rays are impinging on the detector plane. The dispersion time defines the transient range, in which all rays are impinging on the virtual detector plane and is a measure for the signal dispersion. By evaluating the slew rate of the step response, the signal rise time is defined by the switching time from low to high digital level. Furthermore the signal delay time can be defined by T_L, which extends the offset delay time by the time period, required to switch to high digital level. Thus by evaluating this step response, the static and dynamic transfer behavior of the optical waveguide at the detectors position is derived in regard to the applied launch condition and detectors switching capabilities.

4   Numerical results

One important design feature for PCB-integrated optical waveguides is the minimum bending radius. In order to save routing space, small bending radii are preferred. But due to the waveguide bending the optical loss increases with decreasing bending radii. Thus the question arises, which kind of bending radius can be chosen in regard to acceptable bending losses. As the bending losses depend on various waveguide parameters, ray-optical simulation runs are needed, to answer this question. By applying our design technique and our ray-optical simulation tool, the minimum bending radii are determined for different permittivities of the cladding material ϵ_{cl} and different widths w of quadratic core cross sections. In order to isolate the bending losses from other losses, no intrinsic material loss nor surface roughness of the core boundary were considered within the simulation. The applied bended waveguides show circular bended routing section with varying radii $R \in [1, 15]mm$ and constant bending angle of $\pi/2$. In Fig. 6 the simulated bending losses are depicted over the applied bending radius for three different core widths $w = [40, 70, 100]\mu m$. The permittivity of the core material is chosen to be $\epsilon_{co} = 1.253$ and the one for the cladding is $\epsilon_{cl} = 1.245$. As ex-
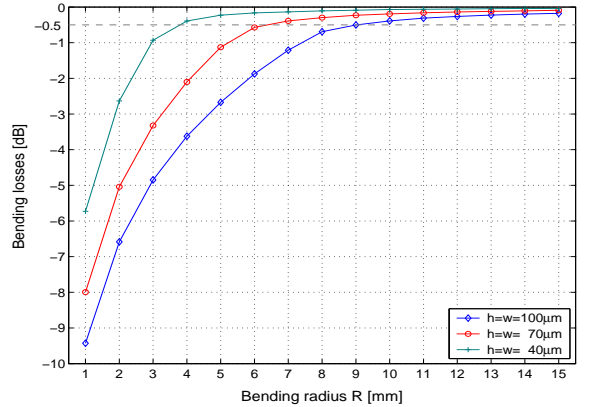

Figure 6: Bending losses for different radii

pected the bending losses are increasing for decreasing bending radius. One remarkable result is that bending losses depend significantly on the width of the core. Smaller transversal core dimensions enable the design of smaller bending radii. This motivates another representation of the bending loss curves. Instead of plotting the bending losses over the radius, they are plotted over the normalized radius R/w in Fig. 7. This leads to another remarkable result. The bending loss curves for different core widths but constant cladding permittivity ϵ_{cl} are lying upon each other. In order to approve this fact, the simulations were repeated for a different cladding permittivity of $\epsilon_{cl} = 1.241$ and its results are additionally depicted in Fig 7. Also for this parameter choice the bending loss curves over the normalized bending radii are lying upon each other confirming the previously obtained result. This result leads to a first design rule for PCB-integrated optical waveguides. The design of waveguide bends has to consider the ratio of bending radius to applied core width of the optical waveguide. An exclusive consideration of the bending

radius without considering the core width is not sufficient for designing optical waveguide bends. Additionally the bending loss curves in Fig. 7 show a strong dependence on the choice of the cladding permittivity, which has to be considered as well within the design of waveguide bends. A typical computing time (Pentium
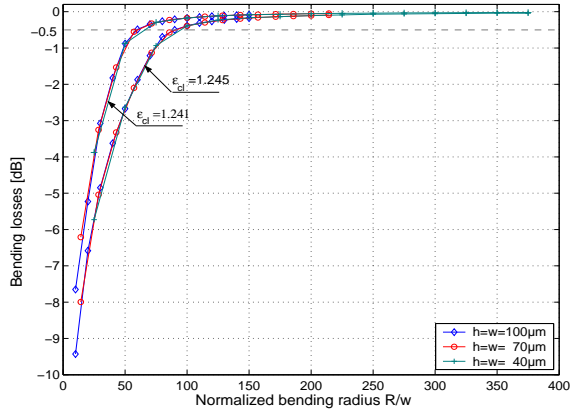

Figure 7: Bending losses for different normailzed radii R/w

4 system) to achieve the above results is ranging from few minutes to few hours depending on the number of initial rays applied (10^3 up to 5×10^6).

5   Conclusion

A novel design technique for PCB-integrated optical waveguides has been introduced. This user-friendly technique supports a likewise novel ray-optical simulation technique with an algebraic description of 3-D boundary geometry of the light guiding core structure of PCB-integrated optical waveguides. Furthermore it offers analytical solutions for ray intersection calculations with the core boundary and thus provides ray-tracing techniques with fast and efficient ray intersection algorithms. Based on ray-tracing algorithm geometrical ray paths traveling along designed core structures can be computed. But this is inadequate for the simulation of the static and dynamic transfer behavior of optical waveguides. Therefore the ray-tracing is extended by an ray-optical simulation technique, that allows the computation of the field energy flow along a geometrical ray-path under consideration of the waveguide's design, the permittivities of applied dielectric material and surface roughness of the core boundary. Under consideration of the spatial emission spectrum of the optical source the signal transmission along optical interconnects is evaluated by computing step responses via virtual detector models.

Applying these techniques, a numerical analysis of the minimum bending radius has been carried out. Here from a first design rule for PCB-integrated optical waveguides has been derived, showing a relationship between bending losses and bending radius normalized to the core width. Furthermore significant dependence of the bending loss behavior on the permittivity of the cladding material has been unveiled. This small simulation example highlights the complexity of designing optical interconnects and emphasizes the need of design and simulation tools for this new optical interchip

interconnect technology.

References

[1] *International Technology Roadmap for Semiconductors.* International Semiconductor Industry Association, 2002.

[2] B. Lunitz et. al. Experimental demonstration of 2.5gbps transmission with 1m polymeroptical backplane. *Electronics Letters*, 37:1079, September 2001.

[3] J. Moisel et. al. Optical backplanes with integrated polymer waveguides. *Optical Engineering*, 39:673–679, March 2000.

[4] Th. Bierhoff et. al. Ray tracing and its verfication for analysis of highly multimode optical waveguides with rough surfaces. *IEEE Transaction on Magnetics*, 37(5):3307–3310, 2001.

[5] L. Dellmann et.al. Polymer waveguides for high-speed optical interconnects. In *EOS Topical Meeting: Optics in Computing*, pages 131–132, Engelberg (Schweiz), April 2004.

[6] M. Karppinen et.al. Embedded optical interconnect on printed wiring board. *SPIE*, 5458:135–145, 2004.

[7] P. Lukowicz et.al. Optoelectronic interconnection technology in the holms system. *IEEE J. Select. Topics Quantum Electron*, 9(2):624, 2003.

[8] F. L. Pedrotti and L. S. Pedrotti. *Introduction to Optics*. Prentice Hall, 1 edition, 1987.

[9] F.P. Schiefelbein and M. Franke. Optical interconnects on printed circuit board level. In *Proc. of the EOS Topical Meeting, Optics in Computing (OC)*, pages 133–143, Engelberg / Switzerland, April 2004.

[10] J. Schrage and Th. Bierhoff. Embedded optical waveguides for on-board interconnections. In *Proceedings Frontiers in Optics, 87th OSA Annual Meeting*, Tucson (Arizona/USA), October 2003.

[11] A. W. Snyder and J. D. Love. *Optical Waveguide Theory*. Chapman and Hall, 4 edition, 1996.